Tuning of Surface Properties of Poly(vinyl alcohol)/ Graphene Oxide Nanocomposites

Camila F. P. de Oliveira,[†] Pablo A.R. Muñoz,[†] Michelle C.C. dos Santos, Gabriela S. Medeiros, Amanda Simionato, Danilo A. Nagaoka, Eunézio A. T. de Souza, Sergio H. Domingues, Guilhermino J. M. Fechine

MackGraphe - Graphene and Nanomaterials Research Center, Mackenzie Presbyterian University, Rua da Consolação, 896, São Paulo, SP, CEP 01302-907, Brazil

Surface properties are extremely important for materials applied in the biomedical areas such as poly(vinyl alcohol)—PVA. The precise control of the surface characteristics on these materials may adjust and expand its applications. Here, we present a new strategy to tune the surface properties of poly(vinyl alcohol)/graphene oxide (PVA/GO) films by manipulation of GO particles (amount and level of oxidation) and also by *in situ* reduction of GO. Adopting a different approach from the methods currently proposed, the reduction process of GO was carried out by exposing the PVA/GO films to hydrazine vapor to maintain the degree of particle dispersion. Raman spectroscopy, contact angle (surface energy), X-ray diffraction, and atomic force microscopy were used to evaluate the interaction between PVA and GO particles and also to characterize graphene polymer composites properties at the surface of the films. The results indicated that there is a strong interaction between the GO particles and polar PVA groups mainly at a very specific stoichiometric ratio. Consequently, the surface properties of the PVA/GO films may be tuned by altering the concentration of the particles, their level of oxidation as well as by the exposure to hydrazine vapor. The impact of these affirmations is extremely important for improving the suitability of PVA in applications such as biomaterial, membranes, packaging, and others that need a rigorous control of surface properties. POLYM. COMPOS., 40:E312–E320, 2019. © 2017 Society of Plastics Engineers

INTRODUCTION

Graphene was first isolated in 2004 by Geim and Novoselov [1]. It is a two-dimensional (2D) structure consisting of carbon distributed in a honeycomb shape, connected via sp^2 bonds. As a result of its structure, graphene has a high surface area, high electronic mobility, and high elasticity modulus, which is much higher than traditional materials, close to 1 TPa. These superlative properties make graphene a candidate that may be applied in several fields such as electronics, communications, and as a reinforcing nanofiller to polymers, promoting new properties, for example, mechanical and electrical [2].

For the development of a polymer nanocomposite, a good dispersion of the nanoparticles in the matrix is essential. Using graphene as reinforcement, agglomerates are usually generated, due to its high specific surface area [3, 4]. Very low load amounts of graphene are needed to achieve the desirable properties of the polymer nanocomposites when compared with usual fillers [5]; however, an extraordinary filler dispersion is a prerequisite for this. Different from manufacturing of electronic devices, the graphene used to produce a polymer nanocomposite has to be obtained using methods with high yields such as liquid exfoliation of graphite [6, 7]. Graphene oxide (GO) and reduced graphene oxide (rGO) are also good candidates to be used as fillers in polymer nanocomposites, as they may also be obtained in relatively large quantities, when compared with mechanical exfoliation [8, 9]. In addition to this, they allow for the possibility of improvements at the polymer-filler interface, in the case of GO, due to the presence of carbonyl groups, hydroxyl and carboxylic acids in the structure [10, 11]. The oxidized groups make GO easily dispersed in polar solvents and may form intercalated nanocomposites with polar polymers through strong secondary interactions [12].

Graphene oxide may be obtained using several modified Hummers methods [13, 14]. In this procedure, more oxygenated groups are produced in the graphite structure, resulting in an insulating material. The graphite oxide (GrO) is the first material produced by the graphite oxidation (Hummers process), this material may also be exfoliated in some solvents, producing very stable isolated graphene

Correspondence to: G.J.M. Fechine; e-mail: guilherminojmf@mackenzie.br

Contract grant sponsor: Fundação de Amparo à Pesquisa do Estado de São Paulo (FAPESP); contract grant numbers: 2012/50259-8, 2015/16591-3; contract grant sponsor: Fundo Mackenzie de Pesquisa (MackPesquisa); contract grant number: 068/2014.

[†]These authors contributed equally to this work.

DOI 10.1002/pc.24659

Published online in Wiley Online Library (wileyonlinelibrary.com).

oxide (GO) dispersion. The GO may be reduced using physical [15–18] or chemical routes [19, 20], yielding a conductive material (rGO).

Poly(vinyl alcohol) (PVA) is one of several polymers used in medical applications due to its excellent biocompatibility, low toxicity, and water absorption [21, 22]. It is also widely used in soft tissue engineering such as artificial collagen for the repair or replacement of cartilage [23, 24]. However, one of the factors limiting its use is its poor mechanical performance, which makes reinforced composites such as PVA with graphene and graphene-like materials (GO and rGO) an interesting solution. As mentioned before, the chemical structures of GO and PVA are very attractive options to create a polymer nanocomposite, as the nanoparticles may be well distributed and dispersed in the polymeric matrix, due to the strong interactions between the oxidized groups of GO and the hydroxyl groups present on the main chain of PVA. Some work related to PVA nanocomposites based on graphene and graphene-like materials have been published in the last 10 years [25–30]. Poly(vinyl alcohol)/graphene oxide (PVA/GO) thin films are prepared by mixing a GO dispersion with a PVA water solution followed by solvent evaporation [28, 30]. Chemical reduction of GO when blended with a PVA water solution, is a strategy used to prepare a PVA/rGO nanocomposite [25, 26]. The direct insertion of rGO particles into the PVA water solution is another way to prepare a PVA/rGO nanocomposite [29], but the amount of rGO in the PVA matrix is limited by the dispersion limit of the particle in water. The main goal of these publications is focused on improvements in the mechanical, thermal, and electrical properties of PVA by inserting GO or rGO particles. However, no assessment of surface characteristics of the nanocomposites was evaluated. Surface properties are extremely important for materials that are applied in the biomedical area such as PVA, mainly hydrophilicity and hydrophobicity. The precise control of the surface characteristics on these materials may adjust and expand its applications.

Here, we present a new strategy to tune the surface properties of PVA/GO films by changing GO amount and its level of oxidation, as well as by *in situ* reduction of GO. Taking a different approach from the methods currently proposed, the reduction process was carried out by exposing the PVA/GO films to hydrazine vapor to maintain the degree of particle dispersion. This new approach of GO reduction overcomes the limitation of rGO concentration in the nanocomposite presented by the methods described before. Raman spectroscopy and X-ray diffraction were used to characterize the graphite oxide, the precursor of GO. Raman spectroscopy, contact angle (surface energy), X-ray diffraction, and atomic force microscopy (AFM) were used to evaluate the polymer nanocomposite properties at the surface of the films. The results obtained clarified how these properties may be tuned according to the desirable application, by changing the filler amount and its chemical structure.

EXPERIMENTAL

Materials

For polymer nanocomposites, PVA from MARCA was used, with $M_W = 10{,}000$ g/mol. The graphite oxide (Gr-O) used to prepare the GO suspensions was produced from natural graphite (Graflake Nacional do Grafite) using a modified Hummers method, as described elsewhere [31]. A water suspension containing 1 mg/mL of GO with an average size of 10 μm and low defect levels was prepared by stirring Gr-O solids in pure water for 3 h, and then sonicating the resulting mixture (ultrasound bath) for 45 min.

Preparation of PVA/GO Nanocomposite

The PVA/GO nanocomposites were prepared to obtain a film 100 micrometers thick. PVA and water were mixed for 30 min at 80°C. Aliquots of graphene oxide (GO) suspension were added to the polymer/water solution to reach the desired concentration. Nine proportions (w/w) of GO in PVA (0%, 0.5%, 1.0%, 1.5%, 2.0%, 5.0%, 10%, 15%, 20%, and 25%) were prepared. The solutions of PVA/water/GO were placed in an ultrasound bath for 20 minutes, for complete homogenization. After homogenizing the solution, it was deposited on a plastic plate and taken to the fume hood until the PVA/GO films formed, after solvent evaporation.

In Situ Reduction of GO

The PVA/GO film was placed inside a glass vessel containing 200 μg of hydrazine solution. The system was heated at 110°C for 6 h, and the hydrazine vapor permeated the PVA/GO nanocomposite films. At the end of this time, the system was turned off. After the inside of the fume hood had reached room temperature, the films were collected.

Characterization

Raman Spectroscopy. Raman spectroscopy analyses of graphite, Gr-O, neat PVA, PVA/GO, and PVA/rGO films were performed on a microscope coupled to a spectroscope Raman scattering, Witec UHTS 300, using a 532 nm laser with1.5 mW power.

Contact Angle. Contact angle tests with water and ethylene glycol were performed in a drop shape analyzer DSA-100 drop (Krüss) at 24°C, to determinate the Surface Free Energy (SFE). The dosing of drops was completed through a manual micrometer control. The contact angles were obtained using the software Advance – Drop Shape, from Krüss. The fitting used for each drop was determined using the best fit observed, and at least twenty measurements were performed for each sample. The SFE

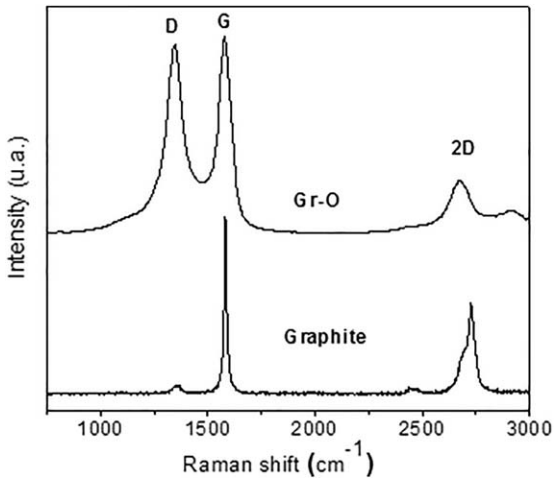

FIG. 1. Normalized Raman spectra of Graphite and Gr—O.

values were calculated using Fowkes methodology. The values of the contact angles (water and ethylene glycol) were used to calculate the surface energy (γ) using an harmonic mean equation [32]. The solution of the equation also gives the values of dispersion (γ_d) and polar (γ_p) components of surface energy.

X-Ray. X-ray diffraction of graphite, Gr-O, PVA/GO, and PVA/rGO films, were performed in a Rigaku diffractometer with K^{α}_{Cu} radiation ($\lambda = 1.42$ Å). The scan range used was from 5° to 70° at a rate scan of 0.083°/s.

Atomic Force Microscopy—AFM. The AFM analyses were made used an ICON ScanAsyst AVH – 1000 from Brucker. A Young's Modulus determination was performed using the Peak Force QNM mode. Sample images of 50 μm × 50 μm were obtained using retrace collected data in the following set up: ScanAsyst Air probe, 256 samples/line, 256 lines, scan rate of 0.8 Hz, room temperature.

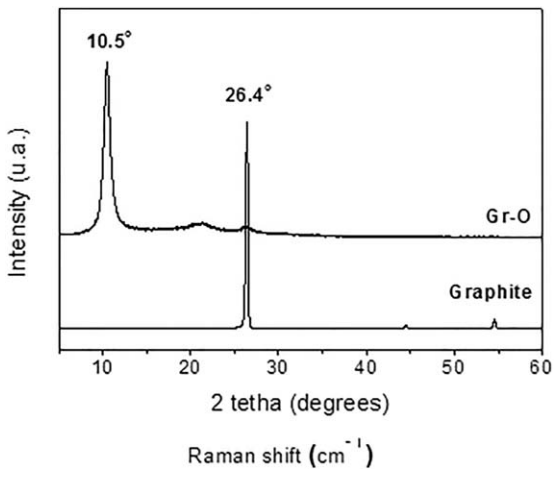

FIG. 2. XRD of Graphite and Gr—O.

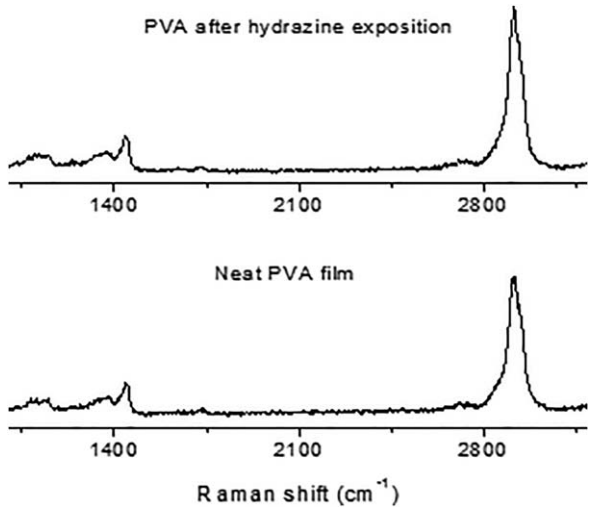

FIG. 3. Raman spectra of PVA film before and after exposure to hydrazine vapor.

All analysis was done after the films be exposed to water-saturated air for up to 48 h to take out the influence of water absorption gradient between the samples.

RESULTS AND DISCUSSION

To confirm the graphene-like structure, the Gr-O was characterized using Raman spectroscopy and X-ray diffraction (XRD). Figure 1 shows a typical Gr-O Raman spectrum, with the 3 different bands described as D (1,345 cm^{-1}), related to the defects in the sp^2 lattice, G (1,580 cm^{-1}), which is correlated to the sp^2 lattice, and 2D (2,700 cm^{-1}), corresponding to the structural organization of the bidimensional lattice in graphene. These same bands may be seen in the graphite spectrum. The oxidation process may be confirmed by the large difference between the two spectra. The increased intensity of the D band in Gr-O is related to the breaking of symmetry in this material when it is oxidized.

XRD measured in a range of 5–60 degrees shows the (002) diffraction peak at $2\theta = 26.4°$ for graphite (Fig. 2). The same band is seen at lower values than 2θ degrees (10.5) for the Gr-O structure. This high shift is attributed to the increase in the graphene layers in Gr-O by the insertion of oxygenated groups [33].

The neat PVA film and composite films of PVA/GO, before and after hydrazine exposition, were all characterized using Raman confocal microscopy, Figs. 3–5, respectively. The Raman spectrum of neat PVA presents two main bands: (1) a band at 1,444 cm^{-1} attributed to the shear mode and (2) a band at 2,915 cm^{-1} attributed to C-H vibrations [34]. These two bands were not affected by the exposure to hydrazine vapor (Fig. 3).

For PVA/GO composites (Fig. 4), G band was stiffened about 15–20 cm^{-1} relative to signal of Gr-O, while the frequency of D band was not affected significantly. The frequency of G band may be tuned by mechanical strains in graphene [35–37], and in the case of blue shift

 DOI 10.1002/pc

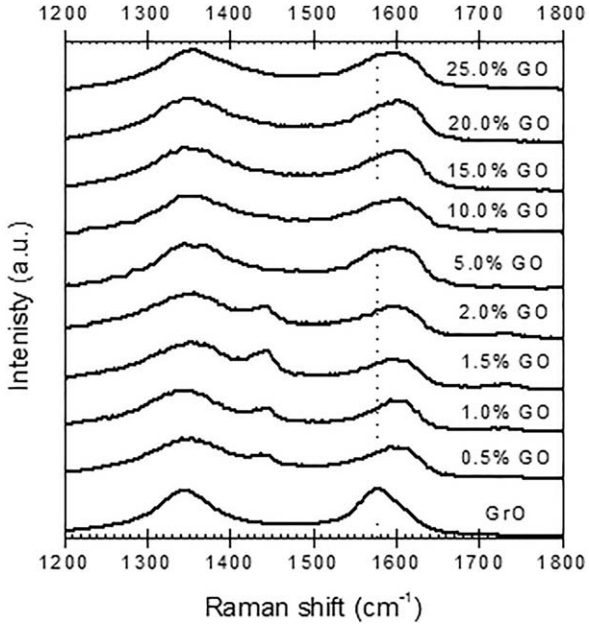

FIG. 4. Raman spectra of PVA/GO composites before hydrazine vapor exposure.

it is due to compressive strain. The shift of G band for graphene-polymer composites may be associated to stretching and compressive strain through an interfacial stress transfer effect [38, 39]. The blue shift of G band observed for PVA/GO composites should be attributed to compressive strain due to PVA crystallization and it may indicate the strong interaction between polymer and GO particles. The ID/IG ratio of the composites is higher ($>$ 1.0) than to Gr-O (0.95), mainly for compositions with low amount of GO. The mixing of PVA and GO was carried out in an ultrasound bath for 20 min, time enough to

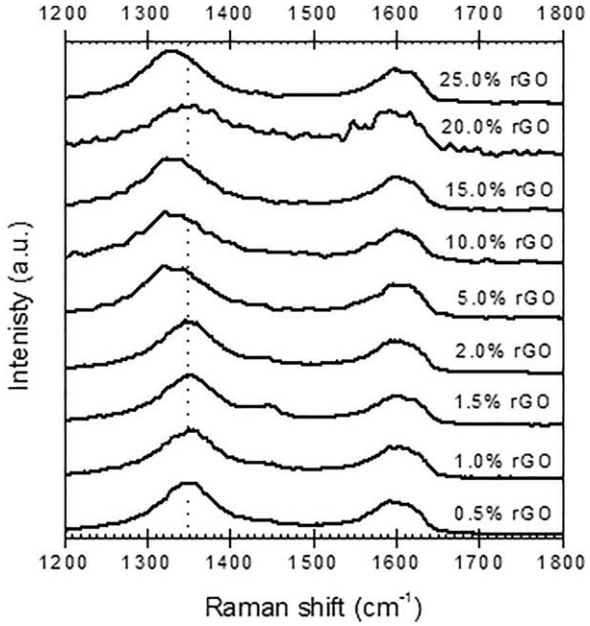

FIG. 5. Raman spectra of PVA/GO composites after hydrazine vapor exposure.

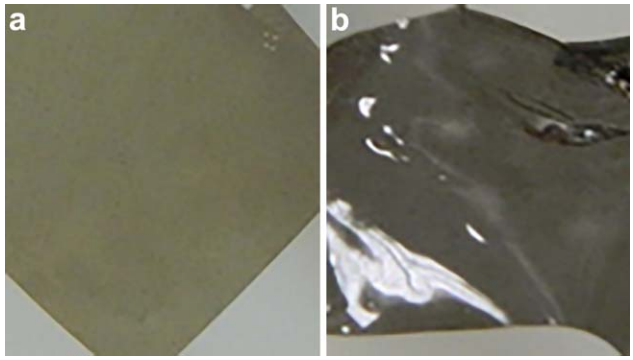

FIG. 6. Images of PVA/GO film with 5.0% (w/w) of filler before (a) and after (b) exposure to hydrazine vapor.

decrease the size of GO particles and increase the ID/IG ratio [40].

The spectra of PVA/GO film after hydrazine exposure (Fig. 5) did not show significant modifications in G band when compared to the spectra before the treatment. However, changes occurred with respect to D band, in intensity and frequency. A red shift of D band is clearly observed for composites with GO amount higher than 5.0%. D band is redshifted when the graphene is subjected to tensile strain [40], indicating that the reduction by hydrazine vapor induced tensile stress at GO particles. The tensile stress could be attributed to oxygenated group removal and deformation of basal plane during the reconstruction. The ID/IG ratio of the composites was increased after the exposure to hydrazine vapor, caused by a decrease in the average size of the sp^2 domains on reduction of the GO [20]. As shown in Fig. 6, the PVA/GO (5.0% w/w) film is light brown before treatment and became very dark after exposure to hydrazine vapor. This phenomenon of color changing is very well known and may also be used to confirm the graphene oxide reduction [41, 42].

Figure 7 shows γ (surface energy) and its polar (γ^p) and dispersive (γ^d) contributive parcels for PVA/GO (Fig. 7a) and PVA/rGO (Fig. 7b). Looking at the data, it is possible to note that there is a significant change in γ up to 1.5% of GO amount, mainly for the PVA/GO composite. As may be seen in Fig. 7a, the decrease in γ is mainly caused by reduction in the polar contributive parcel, which involves a strongly polarized interaction of hydrogen bonds, indicating there are less polar groups at the surface of the film. The interaction between GO oxygenated groups and hydroxyl groups belonging to PVA, probably did not allow the exposure of these polymer polar groups at the surface of the film up to this percentage (1.5%). Figure 8 shows an illustrative sketch with some situations of interactions between GO oxygenated groups and hydroxyl groups that belong to PVA. The neat PVA film shows a great number of hydroxyl groups at the surface, and because of that, the polar contribution is very high (Fig. 8a). However, with the insertion of GO

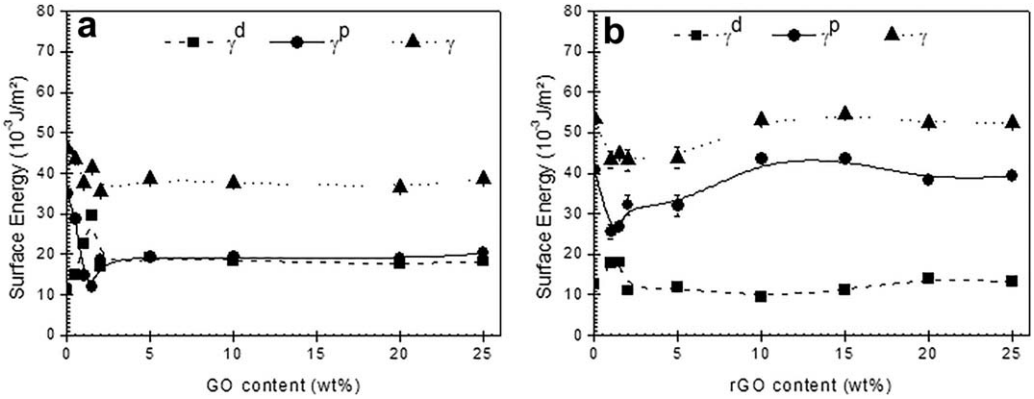

FIG. 7. SFE (γ) and its dispersive (γ^d) and polar components (γ^p) of PVA/GO (a) and PVA/rGO composites (b).

particles (up to 1.5%), interactions between PVA and GO take place as mentioned before, (Fig. 8b) decreasing the polar contribution at the surface of the composite films. A stoichiometric ratio between the oxygenated group of GO and polar PVA groups is probably reached at 1.5% (Fig. 8c) of filler, and after that, the amount of GO drives the interactions. After this point, the amount of GO increases, and the interactions between GO particles were higher than interactions between GO oxygenated groups and polymer polar groups, recovering a certain part of the polar groups at the surface of the film (Fig. 8d). Values of γ, γ^d, and γ^p are partially recovered. A similar behavior has been reported for a GO/PVA composites, where a critical point of percentage of GO (~1.0%) changed significantly the glass transition temperature and mechanical strength of the materials [30]. This phenomenon was also related to the modifications in hydrogen bonding between the GO and PVA matrix. The hydrogen bonding between the GO and PVA matrix increased before the critical point and then decreased, which was the key factor influencing the glass transition temperature. Meanwhile, the mechanical strength of the nanocomposites was improved before the critical point. Matrix increased before the critical point and then decreased, which was the key factor influencing the glass transition temperature. Meanwhile, the mechanical strength of the nanocomposites was improved before the critical point.

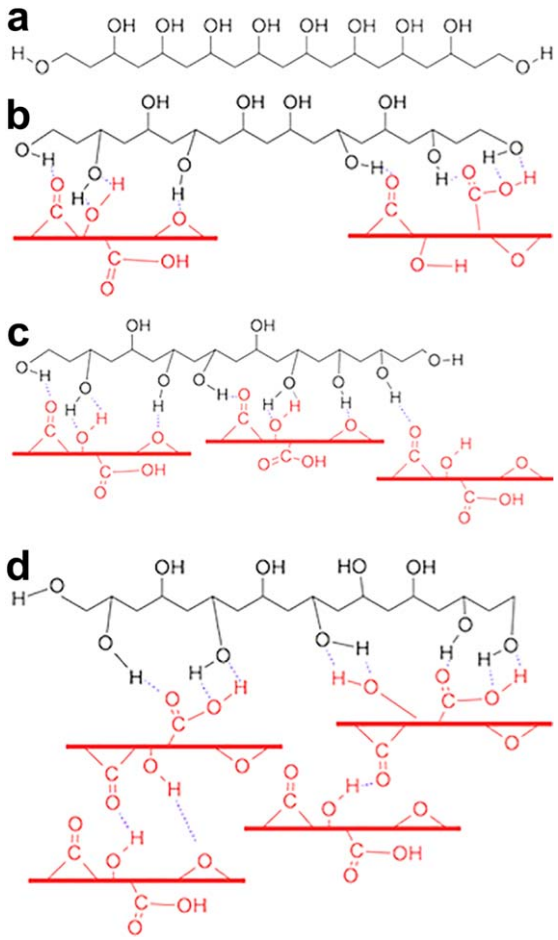

FIG. 8. Illustrative sketch of interactions between GO oxygenated groups and hydroxyl groups belonging to PVA. Hydroxyl groups at surface of neat PVA (a), interactions PVA/GO with amount of GO < 1.5% (b), interactions PVA/GO with amount of GO = 1.5% (c), interactions PVA/GO with amount of GO > 1.5% (d).

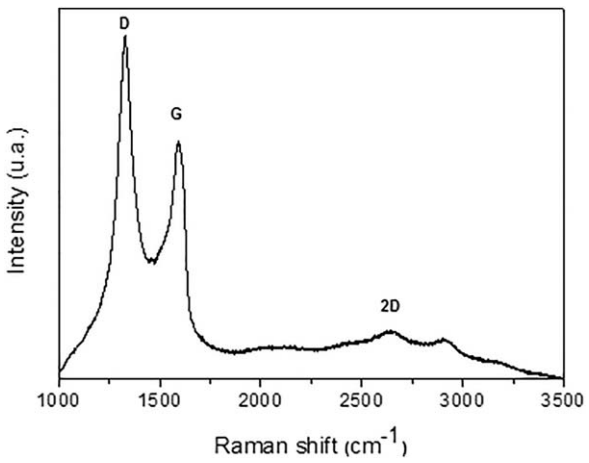

FIG. 9. Raman spectrum of a highly oxidized GO.

DOI 10.1002/pc

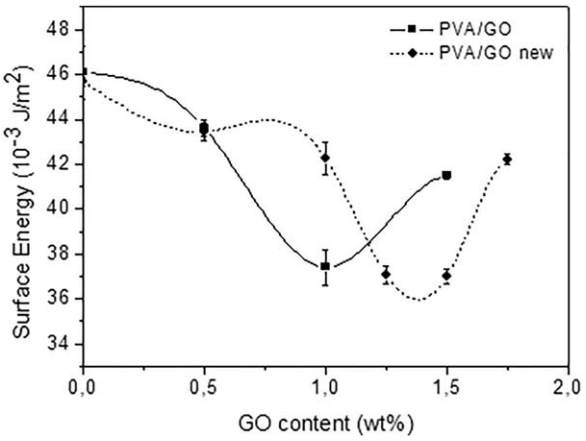

FIG. 10. SFE (γ) of PVA/GO nanocomposites.

To confirm the hypothesis mentioned before, new PVA/GO composites films were prepared using new GO particles with a higher level of oxidation (PVA/GO-new) and SFE data was collected. Figure 9 shows the Raman spectrum of the high-oxidized GO and the three bands ascribed to GO are clearly visible. A D band much more intense than the G band may be due to a very highly oxidized material.

The results presented in Fig. 10 show a minimum surface energy occurring at around 1.0% for the new films, that is, the minimum of γ that happened before the PVA/GO film. These results prove the hypothesis on the existence of a stoichiometric ratio between GO oxygenated groups and polymer polar groups, since new GO particles obtained with a higher number of oxidized groups lead to a lower amount of filler required to reach the saturation point of interactions between GO and the polymer.

After exposure to hydrazine vapor, neat PVA film also presents modifications. The surface energy decreases, due to decreasing polar (γ^p) and increasing dispersive (γ^d) contributive parcels. PVA/rGO composites present higher γ in all ranges of compositions as may be seen on Fig. 7. It happened because the polar interaction between PVA and rGO is weaker than PVA/GO, due to the less number of oxygenated groups in rGO, plus the polymer modification at the surface by the hydrazine vapor. All tendencies for PVA/rGO are quite similar to PVA/GO. However, changes in γ, γ^p, and γ^d are smaller.

The SFE was estimated using a sessil drop test and Fowke's equation. A polar liquid, water, was used. The water contact angles are summarized in Table 1. According to the data presented in Table 1, the presence of GO particles increases PVA hydrophobicity, causing higher contact angles in water drops on top of composite films. Information about hydrophobicity based on the contact angle of the water drop presents the same tendency of the local maximum observed for γ. The maximum PVA/GO hydrophobicity occurs at around 1.5% GO load, where most of the oxygenated groups from GO are probably interacting with PVA hydroxyl groups, as mentioned before. The decrease in hydrophobicity, observed above at 1.5% GO, is probably caused by the strong interaction between GO particles. Above 20% GO the water contact angle decreases significantly, indicating an increase in hydrophilicity. The most likely reason for this is GO crowding or agglomeration, caused by super saturation of the solution used to prepare the films. GO crowding leads to a reduction in the superficial area and the number of exposed oxygenated groups also reduces, thus PVA hydroxyl groups are interaction-free to increase hydrophilicity at the film surface.

The exposure to hydrazine vapor decreased the water contact angle for neat PVA. It is likely that residual water inside the films was removed due to the temperature ($\cong$ 100°C) and time (12 h) of the experiment. PVA/rGO composites show water contact angles higher than neat PVA submitted to treatment with hydrazine, with a load amount up to 1.5%. After this point, the water contact angles decreased to values near neat PVA after treatment. For a low load of filler, there is no particle aggregation, which means the hydrazine can interact strongly with GO particles. The removal of oxygenated groups reduced the interaction with polymer hydroxyl groups, keeping the surface hydrophilic. When the amount of filler increases, the amount of hydrazine is not enough to reduce all GO particles, and the interaction between GO and polymer is stronger, leading to a reduction of polar groups at the film surface, and becoming more hydrophobic.

Figure 11 shows selected PVA and composites diffractograms before (11a) and after exposure to hydrazine vapor (11b). According to the literature, PVA may present several crystalline peaks at 11.5, 16.0, 19.4, 20.0, 22.8, 32.2, and 43° [43]. Neat PVA film before exposure to hydrazine vapor shows a diffractogram with the presence of three remarkable peaks at 19.7, 22.5, and 43°, as well as an immense amorphous hallo. These peaks are related to crystalline planes (101), (200), and (111), respectively. The high temperature used to generate hydrazine vapor acts like a heat treatment, reducing defects in the crystalline net, leading to a better definition of the peaks at 19.7° in addition to decreasing the

TABLE 1. Water contact angles of PVA and composites before and after exposure to hydrazine vapor.

Filler amount (%)	PVA/GO (before) (°)	PVA/rGO (after) (°)
0.0	57.1 ± 0.9	46.8 ± 0.7
0.5	60.3 ± 0.3	61.8 ± 0.9
1.0	76.0 ± 0.5	59.7 ± 0.2
1.5	77.4 ± 0.1	61.0 ± 0.2
2.0	74.5 ± 0.8	62.6 ± 0.4
5.0	70.5 ± 0.4	49.3 ± 0.1
10.0	71.6 ± 0.4	45.9 ± 0.3
15.0	73.0 ± 0.6	47.8 ± 0.3
20.0	70.1 ± 0.5	47.5 ± 0.3
25.0	60.1 ± 0.9	46.8 ± 0.7

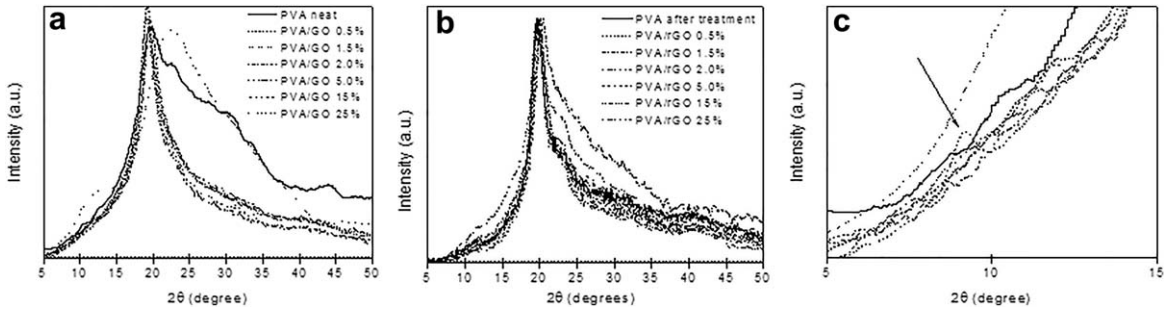

FIG. 11. Diffractograms of PVA and composites before (a) and after exposure to hydrazine vapor (b). Zoom of the region showing diffraction peak of graphite oxide for PVA/GO composite (c).

amorphous hallo. In the case of PVA/GO composites, the GO particles act as a nucleating agent to the polymer, keeping the crystalline characteristics for most compositions, except the composition with 1.5% of GO. For PVA/GO (1.5%), the intensity of the peak localized at 22.5° is increased while the intensity of (101) plane is decreased, changing the crystalline structure of PVA. These results indicate that GO induces a very strong modification in crystalline phases of PVA for this specific percentage, corroborating previous results. As mentioned before, after treatment with hydrazine vapor, the crystalline characteristic of PVA is intensified, and it was also maintained in the composites. For PVA/rGO composites, the diffractograms are very similar for all compositions. The treatment with hydrazine at 110°C induces a restructuring emphasizing the (101) crystalline plane, even for the composite with 1.5% of rGO. However, the peak at 22.5° is still present for all compositions and the composites with 1.5% of rGO show a more intense peak. A similar behavior is found for XRD results, with respect to the values of γ and hydrophobicity, that is, a singular point may be found for the composites.

The characteristic diffraction peak of graphite oxide sheets is observed at $2\theta = 9°$ (Fig. 11c) for PVA/GO composites with a higher amount of filler (25.0%), corresponding to a layer-to-layer distance of 0.98 due to restacking the GO sheets. The PVA/GO composites with GO loadings $< 20.0\%$ exhibit the same diffractograms (except for 1.5% of GO, as explained before), with the absence of the characteristic peak of graphite oxide. This implies that the Gr-O particles in these composites were fully exfoliated into GO as either a single layer or as a few layers in thickness. The peak of graphite oxide sheets cannot be observed for all PVA/rGO composites, even for high loads of rGO. It is probable that during the exposure of hydrazine vapor, an expansion of the sheets occurred due to the evaporation of adsorbed water in the GO sheets, in addition to the reduction.

The mechanical properties of the surface of the films were also investigated to verify possible changes by GO incorporation into PVA, and the effect of hydrazine vapor reduction. The Young's Modulus were measured by AFM, using the Quantitative NanoMechanical (QNM) mode. Collected data was analyzed using Gwyddion free Software and is summarized in Fig. 12.

According to data, there is an increase in the Young's Modulus (E) with an increment in graphitic material amount for PVA/GO and PVA/rGO composites. However, the increase of E in the region between 0.5% and 1.5% is much higher for the PVA/GO composites. The exposure of the films to hydrazine vapor was carried out at 110°C for 6 h, as mentioned earlier. For this reason, the amount of water adsorbed on the surface of the film significantly decreased. It is known that water acts as a plasticizer for PVA, so the increase in the modulus is due to the increase in stiffness of the film surface from the loss of the plasticizer. A decrease in E is observed above 1.5% graphitic percentage, but it increases again near 5% for PVA/GO and 15% for PVA/rGO. Comparing E before and after reduction, a decrease in E for reduced PVA/GO composites is observed. Removing oxygenated groups from GO after the solid-state reduction, leads to a decreased interaction between the graphitic structure and PVA, consequently the adhesion between the polymer and filler decreased, justifying the lower mechanical performance of the PVA/rGO composite.

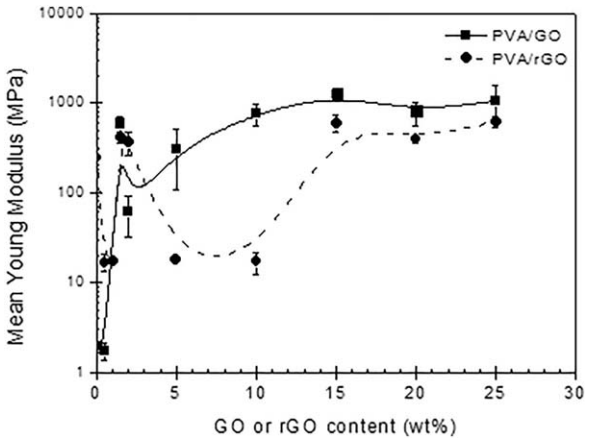

FIG. 12. Young's Moduli at the surface of the films of neat PVA, PVA/GO and PVA/rGO composites.

 DOI 10.1002/pc

CONCLUSIONS

The results of Raman, SFE, water contact angle, X-ray diffraction and AFM, indicated that the surface properties of the films of PVA/GO may be tuned by modifications in the GO amount and level of oxidation obtained during the synthesis of GO particles, as well as by exposure to hydrazine vapor. There is a stoichiometric ratio of oxygenated group of GO particles and polar PVA groups, which may strongly change the interaction between particles and polymer. The exposure of GO particles to hydrazine vapor already inserted into the polymeric matrix does not change the dispersion and distribution of the particles, and it enables the reduction of GO particles, even for high loads. The impact of these statements is extremely important for applications that are already well known for this polymer, such as biomedical, membranes, and packaging and for expansion into several areas that really need the ability to control the PVA surface characteristics.

REFERENCES

1. K.S. Novoselov, A.K. Geim, S.V. Morozov, D. Jiang, Y. Zhang, S.V. Dubonos, I.V. Grigorieva, and A.A. Firsov, *Science*, **306**, 666 (2004). doi:10.1126/science.1102896.
2. J.R. Potts, D.R. Dreyer, C.W. Bielawski, and R.S. Ruoff, *Polymer (Guildf)*, **52**, 5 (2011). doi:10.1016/j.polymer.2010.11.042.
3. S. Gilje, R.B. Kaner, G.G. Wallace, D.A.N. Li, M.B. Mu, M.B. Muller, S. Gilje, R.B. Kaner, and G.G. Wallace, *Nat. Nanotechnol.*, **3**, 101 (2008). doi:10.1038/nnano.2007.451.
4. M.M. Gudarzi, and F. Sharif, *Express Polym. Lett.*, **6**, 1017 (2012). doi:10.3144/expresspolymlett.2012.107.
5. T.K. Das and S. Prusty, *Plast. Technol. Eng.*, **52**, 319 (2013). doi:10.1080/03602559.2012.751410.
6. M. Lotya, Y. Hernandez, P.J. King, R.J. Smith, V. Nicolosi, L.S. Karlsson, F.M. Blighe, S. De, W. Zhiming, I.T. McGovern, G.S. Duesberg, and J.N. Coleman, *J. Am. Chem. Soc.*, **131**, 3611 (2009). doi:10.1021/ja807449u.
7. Y. Hernandez, V. Nicolosi, M. Lotya, F.M. Blighe, Z. Sun, S. De, I.T. McGovern, B. Holland, M. Byrne, Y.K. Gun'Ko, J.J. Boland, P. Niraj, G. Duesberg, S. Krishnamurthy, R. Goodhue, J. Hutchison, V. Scardaci, A.C. Ferrari, and J.N. Coleman, *Nat. Nanotechnol.*, **3**, 563 (2008). doi:10.1038/nnano.2008.215.
8. R. Shah, A. Kausar, B. Muhammad, and S. Shah, *Plast. Technol. Eng.*, **54**, 173 (2015). doi:10.1080/03602559.2014.955202.
9. J. Chen, B. Yao, C. Li, and G. Shi, *Carbon N. Y.*, **64**, 225 (2013). doi:10.1016/j.carbon.2013.07.055.
10. K.P. Loh, Q. Bao, P.K. Ang, J. Yang, *J. Mater. Chem.*, **20**, 2277 (2010). doi:10.1039/b920539j.
11. R.S. Dreyer, D.R. Park, S. Bielawski, and C.W. Ruoff, *Chem. Soc. Rev.*, **39**, 228 (2010). doi:10.1007/978-3-319-15500-5_3.
12. R. Verdejo, M.M. Bernal, L.J. Romasanta, and M. A. Lopez-Manchado, *J. Mater. Chem.*, **21**, 3301 (2011). doi:10.1039/c0jm02708a.
13. S.H. Domingues, R.V. Salvatierra, M.M. Oliveira, and A.J.G. Zarbin, *Chem. Commun. (Camb)*, **47**, 2592 (2011). doi:10.1039/c0cc04304d.
14. H. Mehl, C.F. Matos, E.G.C. Neiva, and S.H. Domingues, *Quim. Nova*, **37**, 1639 (2014).
15. W. Chen, L. Yan, and P.R. Bangal, *Carbon N. Y.*, **48**, 1146 (2010). doi:10.1016/j.carbon.2009.11.037.
16. Y. Zhu, S. Murali, M.D. Stoller, A. Velamakanni, R.D. Piner, and R.S. Ruoff, *Carbon N. Y.*, **48**, 2118 (2010). doi:10.1016/j.carbon.2010.02.001.
17. Y. Zhang, L. Guo, S. Wei, Y. He, H. Xia, Q. Chen, H.B. Sun, and F.S. Xiao, *Nano Today*, **5**, 15 (2010). doi:10.1016/j.nantod.2009.12.009.
18. J. Cao, G.Q. Qi, K. Ke, Y. Luo, W. Yang, B.H. Xie, and M.B. Yang, *J. Mater. Sci.*, **47**, 5097 (2012). doi:10.1007/s10853-012-6383-5.
19. S. Park and R.S. Ruoff, *Nat Nano*, **4**, 217 (2009). doi:10.1038/nnano.2009.58.
20. S. Stankovich, D.A. Dikin, R.D. Piner, K.A. Kohlhaas, A. Kleinhammes, Y. Jia, Y. Wu, S.B.T. Nguyen, and R.S. Ruoff, *Carbon N. Y*, **45**, 1558 (2007). doi:10.1016/j.carbon.2007.02.034.
21. C.C. DeMerlis, and D.R. Schoneker, *Food Chem. Toxicol.*, **41**, 319 (2003). doi:10.1016/S0278-6915(02)00258-2.
22. N. Alexandre, J. Ribeiro, A. Gärtner, T. Pereira, I. Amorim, J. Fragoso, A. Lopes, J. Fernandes, E. Costa, A. Santos-Silva, M. Rodrigues, J.D. Santos, A.C. Maurício, and A.L. Luís, *J. Biomed. Mater. Res. - Part A*, **102**, 4262 (2014). doi:10.1002/jbm.a.35098.
23. A. Karimi, and M. Navidbakhsh, *Mater. Technol. Adv. Perform. Mater.*, **29**, 91 (2014). doi:10.1179/1753555713Y. 0000000115.
24. T. Noguchi, T. Yamamuro, M. Oka, P. Kumar, Y. Kotoura, S. Hyon, and Y. Ikada, *J. Appl. Biomater.*, **2**, 101 (1991). doi:10.1002/jab.770020205.
25. H.J. Salavagione, G. Martínez, and M. A. Gómez, *J. Mater. Chem.*, **19**, 5027 (2009). doi:10.1039/b904232f.
26. X. Yang, L. Li, S. Shang, and X. ming Tao, *Polymer (Guildf)*, **51**, 3431 (2010). doi:10.1016/j.polymer.2010. 05.034.
27. X. Zhao, Q. Zhang, D. Chen, and P. Lu, *Macromolecules*, **43**, 2357 (2010). doi:10.1021/ma902862u.
28. S. Morimune, T. Nishino, and T. Goto, *Polym. J.*, **44**, 1056 (2012). doi:10.1038/pj.2012.58.
29. H.-L. Ma, Y. Zhang, Q.-H. Hu, S. He, X. Li, M. Zhai, and Z.-Z. Yu, *Mater. Lett.*, **102–103**, 15 (2013). doi:10.1016/j.matlet.2013.03.094.
30. G.-Q. Qi, J. Cao, R.-Y. Bao, Z.-Y. Liu, W. Yang, B.-H. Xie, and M.-B. Yang, *J. Mater. Chem. A*, **1**, 3163 (2013). doi:10.1039/c3ta01360j.
31. I.N. Kholmanov, S.H. Domingues, H. Chou, X. Wang, C. Tan, J.-Y. Kim, H. Li, R. Piner, A.J.G. Zarbin, and R.S. Ruoff, *ACS Nano*, **7**, 1811 (2013).
32. R.N. Shimizu and N.R. Demarquette, *J. Appl. Polym. Sci.*, **76**, 1831 (2000). doi:10.1002/(SICI)1097-4628(20000620)76:12 < 1831::AID-APP14 > 3.0.CO;2-Q.
33. L. Stobinski, B. Lesiak, A. Malolepszy, M. Mazurkiewicz, B. Mierzwa, J. Zemek, P. Jiricek, and I. Bieloshapka, *J. Electron Spectros. Relat. Phenomena*, **195**, 145 (2014). doi:10.1016/j.elspec.2014.07.003.

34. C. Wang, Y. Li, G. Ding, X. Xie, and M. Jiang, *J. Appl. Polym. Sci.*, **127**, 3026 (2013). doi:10.1002/app.37656.
35. M.A. Bissett, W. Izumida, R. Saito, and H. Ago, *ACS Nano*, **6**, 10229 (2012).
36. Z.H. Ni, T. Yu, Y.H. Lu, Y.Y. Wang, Y.P. Feng, and Z.X. Shen, *ACS Nano*, **2**, 2301 (2008). doi: dx.doi.org/10.1021/nn800459e.
37. T.M.G. Mohiuddin, a. Lombardo, R.R. Nair, A. Bonetti, G. Savini, R. Jalil, N. Bonini, D.M. Basko, C. Galiotis, N. Marzari, K.S. Novoselov, a. K. Geim, and A. C. Ferrari, *Phys. Rev. B - Condens. Matter Mater. Phys.*, **79**, 205433 (2009). doi:10.1103/PhysRevB.79.205433.
38. D. Wang, X. Zhang, J.W. Zha, J. Zhao, Z.M. Dang, and G.H. Hu, *Polym. (United Kingdom)*, **54**, 1916 (2013). doi: 10.1016/j.polymer.2013.02.012.
39. I. Srivastava, R.J. Mehta, Z.Z. Yu, L. Schadler, and N. Koratkar, *Appl. Phys. Lett.*, **98**, 063102 (2011). doi:10.1063/1.3552685.
40. L.M. Malard, M. a. Pimenta, G. Dresselhaus, and M.S. Dresselhaus, *Phys. Rep.*, **473**, 51 (2009). doi:10.1016/j.physrep.2009.02.003.
41. H. Feng, R. Cheng, X. Zhao, X. Duan, and J. Li, *Nat. Commun.*, **4**, 1539 (2013). doi:10.1038/ncomms2555.
42. V. Lee, L. Whittaker, C. Jaye, K.M. Baroudi, D. A. Fischer, and S. Banerjee, *Chem. Mater.*, **21**, 3905 (2009). doi: 10.1021/Cm901554p.
43. R. Ricciardi, F. Auriemma, C. De Rosa, and F. Lauprêtre, *Macromolecules*, **37**, 1921 (2004). doi:10.1021/ma035663q.